JPPIPA 12(4) (2026)

Jurnal Penelitian Pendidikan IPA

http://jppipa.unram.ac.id/index.php/jppipa/index

Climate-Resilient Vegetation Monitoring in Malang Regency Using Multi-Temporal Remote Sensing

Fatih Al Haq An Nashr Muhsin[1*], Brian Rahardi[1], Estri Laras Arumingtyas[1]

[1] Department of Biology, Faculty of Mathematics and Natural Sciences, Brawijaya University, Malang, Indonesia.

Received: February 09, 2026
Revised: March 15, 2026
Accepted: April 25, 2026
Published: April 30, 2026

Corresponding Author:
Fatih Al Haq An Nashr Muhsin
fatihalhaq4@gmail.com

DOI: 10.29303/jppipa.v12i4.14556

Abstract: Malang Regency exhibits strong topographic and microclimatic contrasts between northern (>500 m) and southern (<500 m), which drive distinct vegetation–climate responses. This study uses MODIS MOD13Q1 NDVI/EVI (February 2000–December 2024), Landsat 8/9 (2013–2024), CHIRPS rainfall, and BMKG stations, processed in Google Earth Engine with cloud masking and compositing, to quantify long-term vegetation trends and vegetation–rainfall relationships. Sen's slope and Mann–Kendall tests indicate significant greening in both zones ($p < 0.01$), with EVI trends steeper than NDVI, reflecting EVI's greater sensitivity to biomass dynamics in high-biomass canopies. Annual EVI–rainfall relationships are stronger in the Southern Zone ($R^2 = 0.545$, $p < 0.001$) than in the Northern Zone ($R^2 = 0.413$, $p < 0.01$), indicating that agro ecosystems in the south remain highly responsive to seasonal rainfall fluctuations despite the presence of irrigation, whereas montane forests are more buffered by groundwater and soil-water storage. ARIMA time-series models provide baseline rainfall scenarios that suggest only a weak downward tendency within historical variability and are interpreted cautiously given the strong influence of ENSO and IOD. These findings offer a quantitative basis for climate-informed land-use planning that simultaneously considers climatic drivers, irrigation management, and ongoing urban expansion in Malang Regency.

Keywords: Climate change; EVI; NDVI; Remote sensing; Vegetation dynamics

Introduction

Climate change is reshaping terrestrial ecosystems by altering temperature and rainfall regimes and, in turn, vegetation dynamics and agricultural production. In tropical regions with pronounced wet–dry seasonality, relatively small shifts in the timing and amount of rainfall can generate large changes in canopy greenness, crop yields, and drought or flood risk (Unsha et al., 2025). Indonesia, as a humid tropical country with high climatic vulnerability, has experienced increasing rainfall variability associated with the El Niño–Southern Oscillation (ENSO), which strongly modulates vegetation condition and agricultural productivity across the archipelago (Liu et al., 2024; Yan et al., 2025).

Malang Regency, covering approximately 3,530 km², exhibits strong topographic and hydroclimatic gradients. The northern highlands (>500 m) are cooler and generally wetter, with annual rainfall exceeding 2,500 mm and landscapes dominated by montane forests and agroforestry systems. In contrast, the lowlands and southern slopes include warmer agricultural zones with 2–3 cropping cycles per year, but some southern districts such as Tirtoyudo, Ampelgading, and Dampit also experience very high rainfall and episodic extreme events driven by orographic uplift from the Semeru massif. This combination of elevation, orographic effects, and east–west rainfall gradients produces sharply contrasting land-cover mosaics and climate–vegetation responses within a relatively small administrative unit, creating a strong need for spatially explicit analysis (Pambudi et al., 2024). Extreme rainfall patterns in southern districts, including Ampelgading, are likely driven by orographic lifting over the Semeru massif. An extensive hydrological study by Marra et al. (2022) demonstrates that the interaction between coastal

How to Cite:
Muhsin, F. A. H. A. N., Rahardi, B., & Arumingtyas, E. L. (2026). Climate-Resilient Vegetation Monitoring in Malang Regency Using Multi-Temporal Remote Sensing. *Jurnal Penelitian Pendidikan IPA*, *12*(4), 442–454. https://doi.org/10.29303/jppipa.v12i4.14556

water vapor flow and steep topography can substantially intensify short-duration extreme precipitation. This mechanism accounts for the persistence of high rainfall in the region during the broader regional dry season.

Satellite remote sensing using vegetation indices such as the Normalized Difference Vegetation Index (NDVI) and Enhanced Vegetation Index (EVI) provides an efficient, cost-effective means to monitor vegetation dynamics over complex terrain (Unsha et al., 2025). NDVI is widely used but saturates at moderate to high leaf area index (LAI), limiting its sensitivity in dense canopies. EVI, which incorporates atmospheric correction and blue-band information, mitigates (rather than completely removes) saturation effects and can retain greater sensitivity at intermediate to high LAI values, although both indices approach asymptotic limits in very dense forests (Xue & Su, 2017; Yan et al., 2025). The availability of long-term, freely accessible archives from MODIS and Landsat, together with cloud-based platforms such as Google Earth Engine, now allows multi-sensor validation and trend analysis of vegetation responses at high spatial and temporal resolution (Meviana & Sari, 2017; Pambudi et al., 2024).

Beyond descriptive trends, robust statistical frameworks are needed to quantify how vegetation indices respond to interannual rainfall variability and to anticipate near-term changes relevant for local planning. Correlation and regression analyses can be used to estimate the sensitivity of NDVI and EVI to rainfall anomalies, while time-series models such as autoregressive integrated moving average (ARIMA) offer a transparent baseline for short-horizon forecasts of rainfall and vegetation indices. Recent work in Indonesia and other tropical regions, however, shows that purely univariate ARIMA models have limited skill under highly volatile hydroclimate conditions and are often extended with exogenous predictors (ARIMAX) or combined with machine-learning approaches such as support vector regression and neural networks to better capture ENSO-related anomalies (Abd-elhamid et al., 2024; Khan et al., 2023). In this study, ARIMA is therefore used as a baseline empirical tool to explore predictability, with explicit recognition that ocean–atmosphere circulation indices (e.g., Niño 3.4) and more complex models are needed for fully operational hydrological planning.

Although global and regional studies have intensively examined vegetation–rainfall relationships, there is still a lack of fine-scale analyses that disentangle agroecological responses between the cool, forested highlands and the heterogeneous, high-rainfall lowland and southern landscapes within Malang Regency (Furusawa et al., 2023; Ramdani et al., 2024). Existing monitoring seldom separates these zones or explicitly evaluates vegetation behaviour during strong ENSO events, despite their importance for local crop calendars and disaster risk management (Mahyuddin & Arif, 2025; Yuniasih et al., 2023).

This research addresses that gap by combining multi-sensor NDVI and EVI time series with rainfall records and ENSO phase information to (i) compare climate–vegetation sensitivities between northern highlands and lowland/southern agroecosystems, and (ii) assess the short-term predictability of vegetation condition using ARIMA-based baselines under varying hydroclimatic conditions. In doing so, the study provides spatially explicit evidence to support climate-sensitive agricultural and land-use planning in one of East Java's key agricultural regencies.

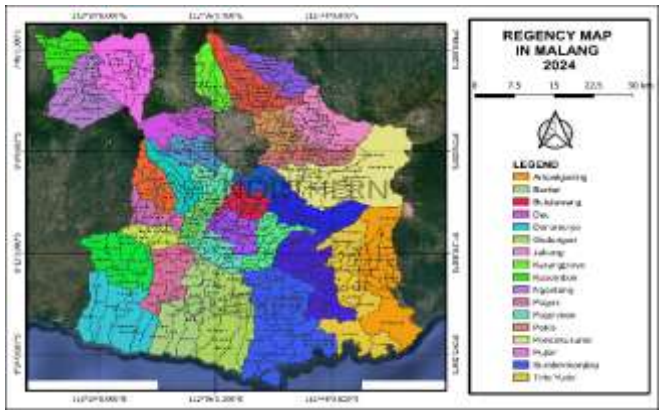

Figure 1. Map of Malang Regency showing northern and southern zones, administrative boundaries, and sampling areas

Method

Study Area

Malang Regency (7°54′41″–8°23′54″S, 112°16′41″–112°57′48″E) spans approximately 3,530 km² with complex volcanic and montane topography. Agroecological zones were delineated using elevation, watershed boundaries, and land-cover transitions. A central contour at 500 m was used to distinguish highland and lowland systems, but a transition band between 400–600 m was explicitly identified and treated cautiously in subsequent analyses to reduce blurring across ecotones. The northern highlands (>500–600 m) are generally cooler and wetter, with annual rainfall often exceeding 2,500 mm and landscapes dominated by montane forests and agroforestry, whereas lowland and southern slopes (<400–500 m) comprise warmer agricultural zones with intensive paddy and mixed cropping systems. Some southern districts, however, also experience very high rainfall and episodic extremes due to orographic uplift from the Semeru massif, reinforcing the need for spatially explicit, zone-based analysis.

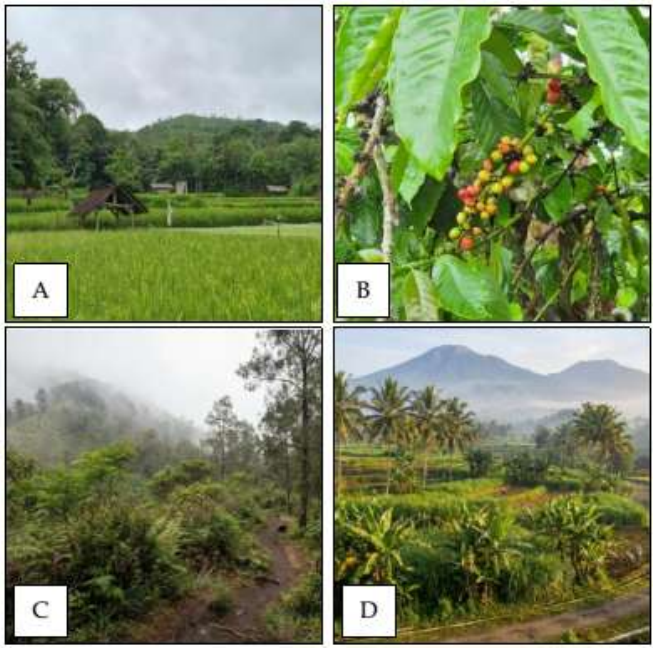

Figure 2. Comparison of vegetation types and local climatic conditions between zones. (A-B) The Southern Zone (Dampit) features an agricultural landscape characterized by paddy fields and coffee plantations. (C-D) The Northern Zone is distinguished by agroforestry systems and mountain forests, with high cloud cover intensity observed in the Bromo Tengger Semeru region

Data Sources

Satellite data comprised MODIS Terra MOD13Q1 Version 6.1 16-day NDVI and EVI composites at 250 m spatial resolution (2000–2024) and Landsat 8/9 OLI surface reflectance products at 30 m resolution (2013–2024). Climate data consisted of CHIRPS gridded rainfall estimates at 0.05° resolution and daily/monthly rainfall observations from BMKG stations within and around Malang Regency. All datasets were accessed and processed in Google Earth Engine, which enabled efficient handling of multi-decadal archives without the need for local high-performance computing.

Data Preprocessing and Cloud Masking

Preprocessing of satellite imagery included cropping to the Malang Regency boundary (Region of Interest, ROI), applying cloud and shadow masking using quality assurance (QA) bands, and generating cloud-reduced composite images. For NDVI and EVI, median compositing was applied over 16-day to monthly windows to suppress residual cloud and haze outliers, producing analysis-ready surface reflectance and vegetation index time series. Geometric correction ensured consistent geolocation across sensors, while atmospheric correction (MOD09/MOD13 and LaSRC for Landsat) minimized effects of scattering and absorption on reflectance values. For rainfall, CHIRPS daily data were aggregated by temporal summation to monthly and annual totals, consistent with the definition of CHIRPS products as total precipitation per period, rather than using median values which would distort volumetric rainfall estimates.

The selection of CHIRPS v2.0 satellite rainfall data for this study is supported by its robust validation record within the study area. Satellite precipitation products were evaluated in the Brantas watershed, demonstrating that CHIRPS effectively captures the spatiotemporal variability of monsoon and orographic rainfall with sufficient accuracy for hydro-climatological assessments (Syaifullah et al., 2025). However, local calibration remains advisable in regions characterized by extreme topography.

Vegetation Index Calculation

The Normalized Difference Vegetation Index (NDVI) was calculated after radiometric and geometric correction using the standard formula: NDVI = (NIR − Red) / (NIR + Red), where Red and NIR denote surface reflectance in the red and near-infrared bands, respectively. NDVI values range from −1 to 1, with higher values indicating denser and healthier vegetation canopies (Belhaj et al., 2025).

The Enhanced Vegetation Index (EVI) was computed as $EVI = G \times (NIR - Red) / (NIR + C_1 \times Red - C_2 \times Blue + L)$, where G is the gain factor, C_1 and C_2 are aerosol resistance coefficients, L is the canopy background adjustment, and NIR, Red, and Blue are surface reflectance in the corresponding bands. Standard MODIS-type coefficients were adopted ($G = 2.5$, $C_1 = 6$, $C_2 = 7.5$, $L = 1$), ensuring consistency with widely used global products unless otherwise stated. Compared to NDVI, EVI mitigates (rather than completely eliminates) saturation in high-biomass conditions and reduces soil and atmospheric background effects, which is particularly relevant for dense agricultural canopies and montane forests in Malang.

Statistical Analysis

Vegetation index and rainfall time series were spatially averaged for each agroecological zone (highland, lowland, and 400–600 m transition band, the latter analysed separately where appropriate). Monthly NDVI and EVI anomalies were computed relative to the 2000–2019 baseline and related to corresponding rainfall anomalies. Pearson correlation coefficients quantified the strength and direction of vegetation–rainfall relationships, while simple and multiple linear regression models estimated the sensitivity (slope) of NDVI and EVI to rainfall variability at monthly and seasonal scales. Model performance metrics (R^2, RMSE) were calculated for each zone to assess differences in climate–vegetation coupling across the landscape.

Cross-Sensor Validation

Cross-sensor validation between MODIS and Landsat was restricted to the overlapping period 2013–2024 using synchronous monthly NDVI and EVI values. To ensure comparable spatial support, Landsat 8/9 30 m vegetation indices were aggregated to the MODIS 250 m grid by averaging all Landsat pixels within each MODIS cell before comparison. Pairwise monthly values from the overlapping period were then used to compute R^2, RMSE, and systematic bias between sensors. Where a consistent linear bias was detected, simple inter-calibration functions (slope and intercept) were estimated and, where necessary, applied to harmonize the series used in regression analysis, thereby reducing artefacts that arise from differences in spatial resolution, spectral response, and atmospheric correction algorithms.

Figure 3. Overall methodological workflow for analysing vegetation–rainfall relationships in Malang Regency. The procedure includes (i) study area zoning based on elevation and agroecological characteristics, (ii) acquisition and preprocessing of MODIS, Landsat, CHIRPS, and BMKG datasets in Google Earth Engine, (iii) computation of NDVI and EVI and zonal time-series extraction, (iv) statistical analysis of vegetation–rainfall relationships and cross-sensor validation, and (v) ARIMA-based baseline forecasting of rainfall for 2025–2027

ARIMA modelling for rainfall prediction (baseline forecasts 2025–2027)

Monthly rainfall time series for each agroecological zone (CHIRPS and station-based) from 2000–2024 were modelled using autoregressive integrated moving average (ARIMA) as a baseline statistical benchmark for short-term predictability. Stationarity was evaluated using the Augmented Dickey–Fuller test, and candidate ARIMA(p,d,q) structures were selected using the auto.arima algorithm based on minimum AIC and diagnostic checks on residuals. Instead of a single 80–20 split centred on 2021–2024, model skill was assessed via rolling-origin time-series cross-validation and hindcasts of key anomalies, including the strong El Niño of 2015–2016 and the recent multi-year La Niña episodes around 2020–2023, which substantially increased rainfall over many parts of Indonesia. This design reduces bias arising from training only on "normal" years and testing exclusively on anomalously wet years. Forecasts for 2025–2027 are thus interpreted as ARIMA-based baseline scenarios, with explicit recognition that actual rainfall outcomes will depend on future ENSO/IOD conditions that are not fully captured by univariate models (Iskandar et al., 2023).

Result and Discussion

Results

NDVI and EVI trends (2000–2024)

Trend analysis of MODIS-derived vegetation indices for 2000–2024 revealed significant greening in both Southern and Northern Zones (Gao et al., 2022; Ramdani et al., 2024; Wingate et al., 2019). All combinations of zone and index exhibited positive Sen's slopes with statistically significant Mann–Kendall test results, although the magnitude of the increase varied (Table 1). EVI trends were steeper than NDVI trends, with EVI increasing by approximately +5.7% to +8.1% compared to NDVI increases of +1.8% to +2.3%, indicating stronger apparent sensitivity of EVI to structural and physiological changes in vegetation canopies (Yan et al., 2025). The Southern Zone showed the largest change, with EVI rising by about 8.1% over the study period ($p = 0.0008$). This pattern is consistent with intensification of irrigated agriculture, expansion of paddy fields, and improved crop management in lowland areas, which collectively raise canopy biomass and greenness. By contrast, the Northern Zone showed a more moderate EVI increase of about +5.7% ($p = 0.0032$), attributed to a combination of natural forest recovery, reforestation, and reduced anthropogenic pressure in some upland areas (Arjasakusuma et al., 2020; Sadiq et al., 2025).

Table 1. Mann–Kendall Trend Statistics and Sen's Slope for NDVI and EVI (2000–2024)

Zone	Index	Sen's Slope	P-value	Interpretation
Northern	NDVI	+1.8%	0.0245	Moderate increase
Northern	EVI	+5.7%	0.0032	Strong increase
Southern	NDVI	+2.3%	0.0089	Moderate increase
Southern	EVI	+8.1%	0.0008	Strong increase

Coefficient of variation values showed that EVI was more variable (CV ≈ 7.1–7.3%) than NDVI (CV ≈ 4.2–4.4%) in both zones. Part of this higher variability reflects genuine responsiveness of EVI to changes in canopy structure and phenology, but it also includes increased sensitivity to view–sun geometry and residual atmospheric effects associated with the blue band, so the additional variability cannot be interpreted solely as improved vegetation sensitivity (Xue & Su, 2017). Spatial maps of 5-year mean NDVI and EVI demonstrated that the northern highlands consistently maintained high greenness values associated with dense forests, whereas the southern lowlands exhibited high but more spatially heterogeneous greenness related to agricultural mosaics (Trevisiol et al., 2024).

Figure 4. Time series plot of NDVI and EVI (2000–2024) for both northern and southern zones

Interestingly, mean NDVI and EVI values were systematically higher in the Southern Zone than in the Northern Zone throughout 2000–2024. Average NDVI in the South (≈0.699) exceeded that in the North (≈0.661) by about 5.7%, and average EVI in the South (≈0.450) was about 10.6% higher than in the North (≈0.407). Although annual mean NDVI and EVI values appeared slightly higher in the Southern Zone than in the Northern Zone, this pattern is likely influenced by methodological factors rather than indicating that agricultural mosaics consistently exceed dense montane forests in true canopy greenness. In the Northern Zone, multi-layered forest canopies with high LAI push NDVI towards its asymptotic regime and increase the risk of residual cloud and haze contamination, both of which compress the dynamic range of indices even when biomass remains high (Ramdani et al., 2024; Rustanto & Booij, 2022). In contrast, lowland croplands often occupy

clearer-sky areas and exhibit single-layer canopies with LAI within the more linear response range of NDVI and EVI, so that their phenological peaks are captured more sharply in satellite composites (Lykhovyd et al., 2024). Consequently, the South–North differences in mean index values should be interpreted cautiously as composite- and sensor-driven artefacts, while the more robust signal lies in the consistent positive greening trends observed in both zones.

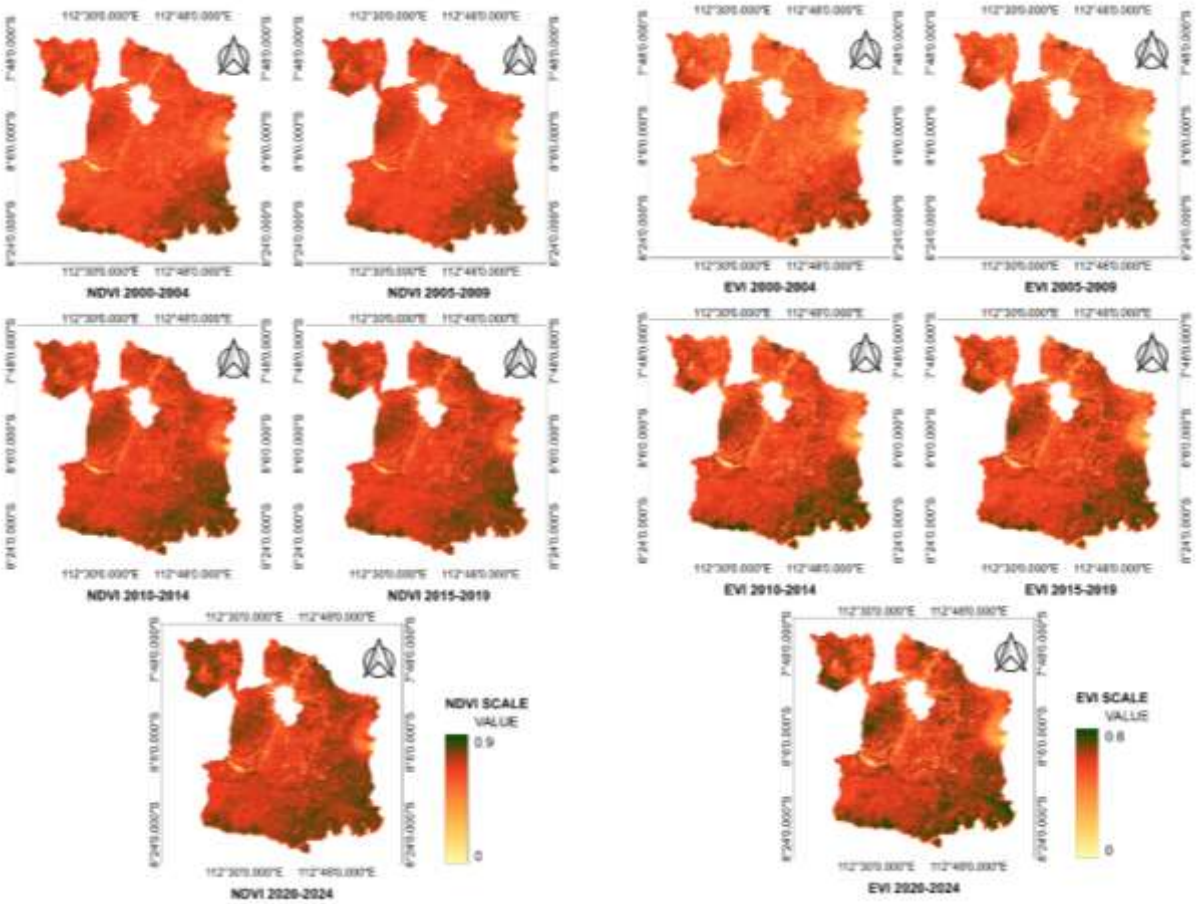

Figure 5. Spatial maps showing 5-year mean NDVI and EVI (2000–2024) for both zones, illustrating spatial patterns of greenness

In contrast, paddy fields and other crops in the Southern Zone typically exhibit single-layer canopies with LAI in the 2–4 range, where NDVI and EVI remain within their more linear response domains and are highly responsive to cropping-cycle dynamics. The occurrence of two to three cropping cycles per year produces temporally synchronised peaks in greenness at the landscape scale, enhancing mean annual indices. Additionally, lower cloud persistence in the Southern Zone improves data quality and reduces atmospheric damping of vegetation signals (Rustanto & Booij, 2022).

ENSO-Related Anomalies: the 2019 El Niño

During the 2019 El Niño, annual rainfall deficits of roughly 24–30% were accompanied by negative NDVI and EVI anomalies of about −3 to −6%, with larger declines in parts of the Southern Zone, consistent with broader reports of vegetation stress during recent El Niño events in Indonesia (Mahyuddin & Arif, 2025; Yuniasih et al., 2023). Spatial inspection suggests that the strongest vegetation stress signals are concentrated in rain-fed and dryland areas, whereas irrigated schemes buffered much of the rainfall deficit through reservoir and canal management. Consequently, the zone-average anomaly of about −4.5% for NDVI should be interpreted as a composite of relatively stable irrigated lowlands and more vulnerable upland drylands, rather than as uniform stress across all agricultural systems supplied by large reservoirs such as Karangkates.

In the Northern Zone, NDVI dropped by roughly −3.24% and EVI by −5.51%, indicating moderate vegetation stress but with some buffering capacity likely provided by deep root systems and higher soil-water storage in montane forests (Arjasakusuma et al., 2020). In the Southern Zone, NDVI decreased by about −4.52% and EVI by −5.16%, revealing a stronger sensitivity of

agricultural vegetation to rainfall deficits (Le, 2023). Irrigated and rain-fed crops in the lowlands are directly dependent on seasonal water availability, and reduced rainfall can quickly translate into lower canopy biomass and greenness, especially in areas where irrigation infrastructure is incomplete or highly constrained (Lykhovyd et al., 2024).

Table 2. Anomaly Indices during 2019 El Niño Event

Zone	NDVI (%)	EVI (%)	Rainfall anomaly (%)	Interpretation
Northern	-3.24	-5.51	-26.2	Moderate stress; buffering effect
Southern	-4.52	-5.16	-29.8	Strong stress; direct impact on crops

Relationships between Vegetation Indices and Rainfall

Linear regression between annual NDVI and annual rainfall highlighted distinct behaviours in the two zones. In the Northern Zone, the NDVI–rainfall relationship was positive but moderate, with R^2 around 0.23 and a Pearson correlation coefficient of about 0.48 ($p < 0.05$). This indicates that only about 22–23% of NDVI variance is explained by rainfall, and that other factors such as soil-water storage, forest structure, and management practices play substantial roles (Li et al., 2021; Uribe et al., 2021). The regression slope suggested a relatively low sensitivity of NDVI to rainfall changes, consistent with the buffering capacity of montane forests and volcanic soils, which store water and sustain greenness during short-term rainfall deficits.

In the Southern Zone, the NDVI–rainfall relationship was notably stronger, with R^2 around 0.39 and a correlation of about 0.62 ($p < 0.01$). Approximately 39% of NDVI variance was thus attributable to rainfall variability (Safa et al., 2021; Pratiwi & June, 2023). The regression slope indicated higher sensitivity of NDVI to changes in annual rainfall, reflecting the dependence of irrigated and rain-fed crops on water availability, particularly in systems where irrigation infrastructure is incomplete or vulnerable to supply fluctuations (Boubaker & Rabah, 2023; Rustanto & Booij, 2022).

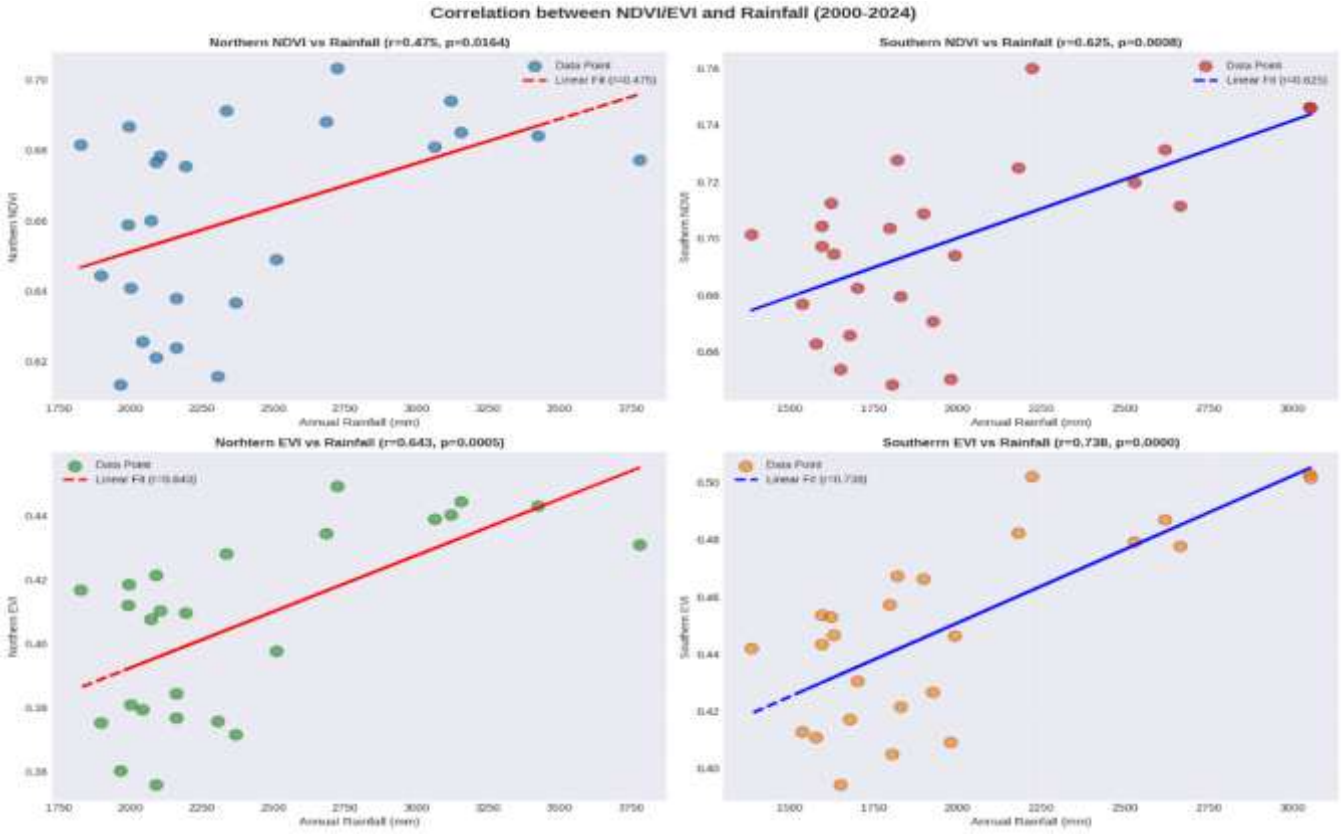

Figure 6. Scatter plots of EVI vs annual rainfall for Northern and Southern zones (2000–2024) with linear regression fits and R^2 values

These results suggest that, in this study area, EVI generally provides a more responsive indicator than NDVI for climate-related vegetation variations, while also being more sensitive to viewing and atmospheric conditions (Xue & Su, 2017; Yan et al., 2025). The greater responsiveness arises from EVI's use of blue reflectance

and correction factors that reduce soil and atmospheric effects and mitigate saturation at high LAI, although these same properties can increase sensitivity to solar geometry and residual atmospheric noise (Naicker & Mutanga, 2024). Cross-sensor comparisons showed that, after aggregating Landsat 8/9 indices to the MODIS grid and restricting the analysis to 2013–2024, both sensors produced broadly consistent climate–vegetation relationships. In the Northern Zone, EVI–rainfall regressions yielded R^2 values of approximately 0.41, while NDVI–rainfall models were weaker ($R^2 \approx 0.23$), with only modest differences between MODIS and Landsat versions of each index. These results suggest that, although Landsat's finer spatial resolution offers advantages for mapping small-scale heterogeneity, MODIS remains adequate for capturing zone-scale vegetation–rainfall coupling over multi-decadal periods (Trevisiol et al., 2024; Rustanto & Booij, 2022).

Table 3. Linear Regression Statistics: Vegetation Indices vs Annual Rainfall

Zone	Index	Intercept	R^2	Pearson r	P-value
Northern	NDVI	0.5900	0.2257	0.4751	0.0164*
Northern	EVI	0.3400	0.4100	0.6403	0.0005**
Southern	NDVI	0.5900	0.3905	0.6249	0.0008**
Southern	EVI	0.3100	0.5450	0.7380	<0.0001***

Note: Asterisks indicate statistical significance levels: * $p < 0.05$, ** $p < 0.01$, *** $p < 0.001$.
NDVI: Normalized Difference Vegetation Index; EVI: Enhanced Vegetation Index.

ARIMA-Based Climate and Vegetation Projections

ARIMA models fitted to 2000–2024 monthly rainfall series suggested a weak downward tendency in annual totals over the next few years, but with wide confidence intervals that encompass both wetter- and drier-than-average outcomes (Abd-elhamid et al., 2024; Khan et al., 2023). Point forecasts indicated modest decreases on the order of a few percent relative to recent means; however, these values should be interpreted as baseline statistical scenarios rather than precise predictions, because ARIMA does not explicitly incorporate non-stationary drivers such as ENSO and the Indian Ocean Dipole that strongly modulate rainfall in East Java. From a climatological perspective, the main message is that substantial interannual variability will likely persist, so planning should be based on a range of plausible wet and dry conditions rather than a single deterministic trajectory (Kliengchuay et al., 2025; Waqas & Thandar, 2024).

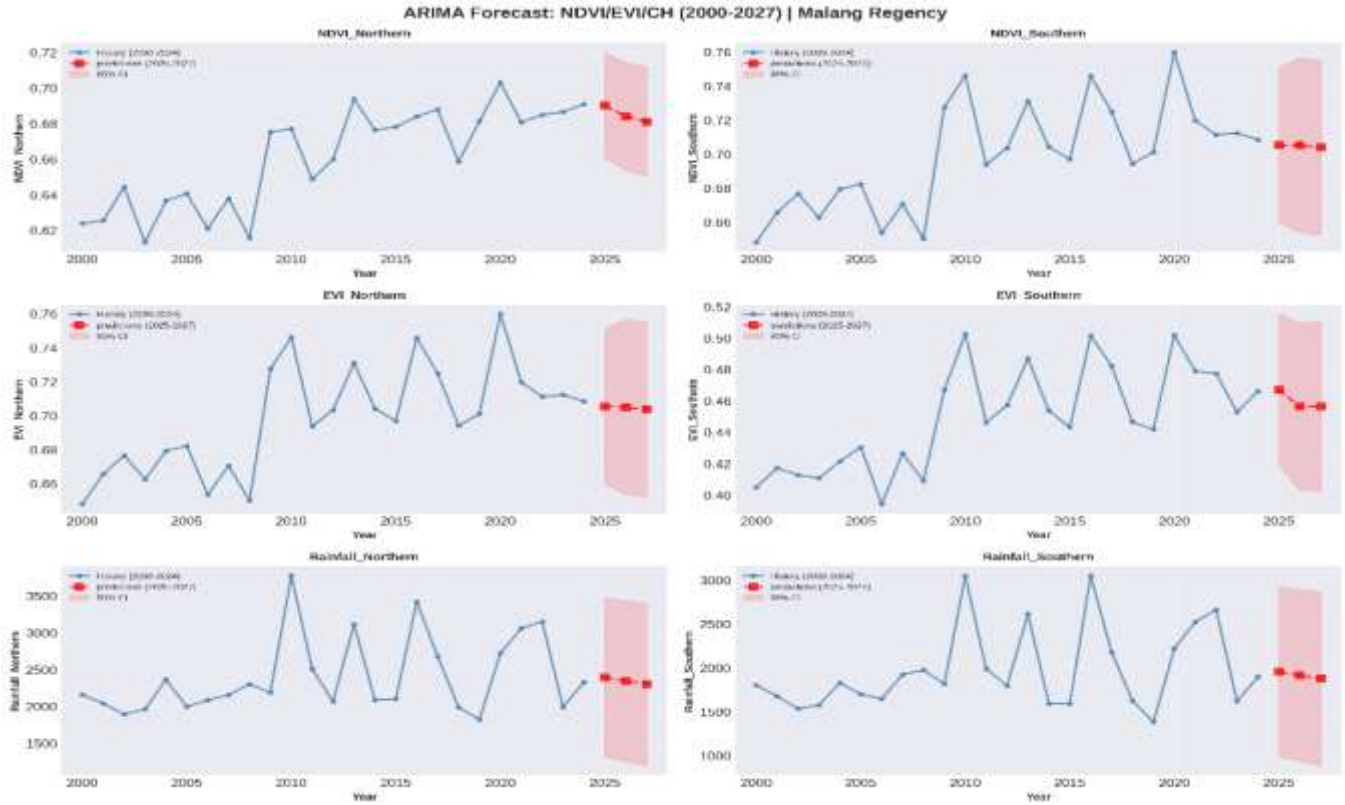

Figure 7. ARIMA rainfall forecasts (2025–2027) for northern and southern zones with 95% confidence intervals

The ARIMA model employed in this study serves as a statistical baseline. However, univariate models are limited in their ability to capture the nonlinearity of tropical rainfall volatility. A recent comparative study in East Java by Permata et al. (2024) demonstrates that hybrid or machine learning approaches, such as Support Vector Regression (SVR), achieve higher prediction accuracy than standard ARIMA models, particularly for forecasting extreme rainfall events.

Despite the downward tendency, the 95% confidence intervals for these forecasts were relatively wide, reflecting the inherently high variability of tropical rainfall. This implies that while a modest drying tendency is plausible, substantial interannual fluctuations remain likely, and individual years could still be wetter or drier than the long-term mean. Time-series models applied to NDVI and EVI suggested that vegetation greenness is likely to remain relatively stable in the near term, with projected NDVI values generally in the range of 0.65–0.71 and corresponding high EVI values indicating sustained green and productive vegetation. The stability of these projections reflects the combination of gradual climatic change and adaptive land management, as well as the dampening effect of soil and groundwater storage, which buffer vegetation against short-term rainfall fluctuations, especially in the northern highlands (Wingate et al., 2019; Sadiq et al., 2025).

Discussion

Differential Vegetation Responses

Results reveal distinct vegetation dynamics between northern highlands and southern lowlands despite both showing long-term greening. The Southern Zone's higher vegetation indices despite lower rainfall reflect canopy structure differences: southern paddy fields have single-layer canopies (LAI 2–4) where NDVI/EVI remain in near-linear response ranges, whereas northern montane forests have multilayered canopies (LAI >3–4) that drive NDVI towards saturation and reduce apparent sensitivity. Multiple cropping cycles per year in the south produce synchronised phenological peaks, enhancing mean indices, while persistent cloud cover and complex topography in the north can dampen observed greenness signals even in intact forests (Ramdani et al., 2024; Wingate et al., 2019). These factors help explain the apparent paradox and underscore the importance of accounting for land-cover composition and sensor limitations when interpreting vegetation indices.

Climate adaptation strategies must be tailored to zone-specific conditions. Southern agricultural systems require robust water-management and drought-mitigation measures, including improved irrigation scheduling and diversification of cropping systems. Northern forested areas need sustained protection and careful management to maintain their hydrological buffering capacity and role in stabilising downstream water supply (Sadiq et al., 2025).

Both climatic factors and significant anthropogenic pressures influence vegetation dynamics in Malang. Recent research documented a rapid shift from a diffusion phase to a coalescence phase in urban sprawl patterns within peri-urban areas of Malang, including Singosari and Pakis (Hafiz et al., 2025). The transformation of productive agricultural land into built-up areas generates a pronounced local 'browning' signal, which should be differentiated from the 'greening' trend associated with climate variability.

The ecological consequences of vegetation loss are measurable. A concurrent study in Malang City demonstrated vegetation's thermal buffering capacity, showing that a 0.1 decrease in NDVI is associated with a 0.339°C increase in Land Surface Temperature (LST). In contrast, an increase in built-up density (NDBI) raises temperatures by over 1°C (Hasyim et al., 2025). These findings indicate that the observed 'browning' in peri-urban districts such as Singosari not only reflects biomass loss but also signals an expanding Urban Heat Island (UHI) risk into the regency's agricultural buffers.

ENSO Impacts and Early-Warning Potential

The 2019 El Niño analysis confirms ENSO's strong influence on rainfall and vegetation in Malang Regency, with rainfall deficits of 24–30% and vegetation declines of 3–6% that align with broader tropical patterns (Le, 2023; Mahyuddin & Arif, 2025; Yuniasih et al., 2023). The stronger southern impact underscores agricultural vulnerability to hydroclimatic extremes, particularly in rain-fed and marginal lands. Given ENSO's interannual predictability and satellite monitoring capabilities (e.g., EVI thresholds below about 0.45 indicating heightened drought risk), there is substantial potential to develop early-warning systems for agricultural drought that integrate ENSO-based rainfall forecasts with satellite-derived vegetation indices (Johnson et al., 2021; Raj & Gopikrishnan, 2023). Such systems could provide 2–4 weeks' lead time for planting adjustments and water-allocation decisions, helping to reduce crop failure risk during ENSO events.

The impact of ENSO is not uniform across regions. The 2023 El Niño event exhibited a distinct 'dipole' pattern in the Maritime Continent. According to Zehri et al. (2025), northern Indonesia experienced increased rainfall. In contrast, southern regions, including Java and Malang Regency, experienced severe rainfall deficits due to the combined effects of a positive Indian Ocean Dipole (IOD) and monsoon circulation anomalies. These conditions account for the marked decline in

vegetation productivity observed in the Southern Zone at the conclusion of the study period.

The cross-correlation analysis indicates a delayed vegetation response to rainfall anomalies. This finding aligns with the characteristics of drought propagation in Java, where meteorological droughts typically precede agricultural droughts, specifically soil moisture deficits, by approximately two to three months, as reported in the 2023 drought impact study by Arifin et al. (2025). This insight is essential for developing effective early warning systems.

Utility of EVI and Remote Sensing Integration

In the Southern Zone, EVI–rainfall relationships reached R^2 values up to about 0.545, indicating a relatively strong coupling between vegetation greenness and seasonal water availability, while in the Northern Zone the coupling was weaker but still significant. However, in irrigated rice systems this coupling is mediated by human decisions, including irrigation scheduling, reservoir operations, and seed distribution policies, which are themselves aligned with the onset and progression of the rainy season. The high correlations therefore reflect the combined effect of rainfall and water-management practices following the seasonal cycle, rather than a purely direct biophysical response to rainfall alone.

EVI consistently captured climate-related variations in vegetation more strongly than NDVI, especially in high-biomass and cloud-affected environments, but also exhibited higher sensitivity to viewing and atmospheric conditions (Xue & Su, 2017; Naicker & Mutanga, 2024). Integration of satellite-derived EVI with local agricultural knowledge and decision frameworks could support more climate-sensitive management of planting calendars and irrigation strategies in Malang and similar tropical regions.

The pronounced sensitivity of agroecosystems in the Southern Zone to rainfall anomalies aligns with observations from adjacent regions. In Bondowoso District, it was reported that during the 2023 El Niño event, rainfed agricultural land experienced significant thermal stress and a notably greater decline in vegetation vigor than plantation areas (Suud & Kusbianto, 2024). These findings further demonstrate the vulnerability of seasonal agricultural systems on the southern slopes of Java to climate shocks.

Strengths, Limitations, and Future Directions

The use of long-term MODIS and Landsat archives, processed in GEE with rigorous cloud masking and compositing, is a major strength of this study. It allows consistent, multi-decadal analysis of vegetation–climate interactions over a complex tropical landscape without the need for local high-performance computing resources. The integration of station and gridded rainfall data further enhances the robustness of climate–vegetation relationships (Berra et al., 2024; Rustanto & Booij, 2022). Nevertheless, several limitations should be acknowledged. First, while optical satellite data remain highly effective for vegetation monitoring, some periods—especially during prolonged cloudy conditions—may experience reduced data availability or residual cloud contamination despite rigorous cloud masking protocols; however, high-frequency acquisitions and compositing mitigate much of this issue (Trevisiol et al., 2024). Second, the zonal aggregation used in the analysis may obscure sub-regional heterogeneity within each zone, such as differences between specific catchments, land uses, or management regimes (Meviana & Sari, 2017; Pambudi et al., 2024).

Third, the ARIMA-based rainfall projections, while informative as short-term baselines, carry substantial uncertainty and cannot capture all potential drivers of future climate change, including global warming and changes in large-scale circulation patterns beyond the historical record (Kliengchuay et al., 2025; Waqas & Thandar, 2024). Future work could address these limitations by incorporating additional variables such as land-surface temperature, soil moisture, and solar radiation (Raj & Gopikrishnan, 2023); by using more spatially disaggregated analyses (Sadiq et al., 2025); and by exploring non-linear or machine-learning models that may capture more complex relationships between climate drivers, vegetation indices, and land-use factors (Johnson et al., 2021). More extensive field data collection, including systematic LAI measurements and soil characterisation, would also improve the validation and calibration of remotely sensed indices and models (Wingate et al., 2019).

Conclusion

Remote sensing analysis shows a statistically significant overall greening signal in Malang Regency between 2000 and 2024, with stronger EVI than NDVI trends, but this increase is dominated by agricultural and upland green cover and co-exists with localised vegetation loss in rapidly urbanising corridors such as toll-road exits and peri-urban settlements. Vegetation–rainfall relationships differ markedly between zones: southern agroecosystems exhibit higher apparent rainfall sensitivity (EVI $R^2 \approx 0.55$, $p < 0.001$) than northern montane forests (EVI $R^2 \approx 0.41$, $p < 0.01$), reflecting the dominance of annual crops in the south that respond quickly to seasonal rainfall anomalies, while upland forests are buffered by deep soils and groundwater storage. ARIMA-based forecasts indicate only a weak downward tendency in annual rainfall over

2025–2027, on the order of a few percent and well within historical variability, and are interpreted as baseline scenarios rather than precise predictions given the strong influence of ENSO and IOD that is not explicitly modelled. Overall, the results highlight that climate variability and human land-use decisions jointly shape vegetation dynamics in Malang, suggesting that climate-informed adaptation must be coupled with careful regulation of urban expansion, protection of montane forests, and resilient irrigation management in southern agricultural zones. Future research should incorporate explicit land-use change layers, field-based measurements of LAI and soil properties, and multivariate or machine-learning time-series models that include ENSO/IOD indices to better separate climatic from anthropogenic drivers and to improve near-term early-warning capability for drought and crop failure.

Acknowledgments
This research is part of the first author's thesis in the Master Program of the Faculty of Mathematics and Natural Sciences, Brawijaya University, Malang, Indonesia.

Author Contributions
F. A. H. A. N. M. contributed to research, data analysis, and article writing; B. R., E. L. A., as a supervisor in research activities until article writing.

Funding
This research received no external funding.

Conflicts of Interest
The authors declare no conflict of interest.

References

Abd-Elhamid, H. F., El-Dakak, A. M., Zeleňáková, M., Saleh, O. K., Mahdy, M., & Abd El Ghany, S. H. (2024). Rainfall forecasting in arid regions in response to climate change using ARIMA and remote sensing. *Geomatics, Natural Hazards and Risk*, *15*(1), 2347414. https://doi.org/10.1080/19475705.2024.2347414

Arifin, Y., Maharani, Y. N., & Cahyadi, T. A. (2025). Analysis of Meteorological–Hydrological Drought Propagation for the Development of a Drought Early Warning System in the Special Region of Yogyakarta (DIY): A Case Study of the 2023 El Niño Event. *International Journal of Current Science Research and Review*, *08*(12), 6414–6426. https://doi.org/10.47191/ijcsrr/V8-i12-52

Arjasakusuma, S., Mutaqin, B. W., Sekaranom, A. B., & Marfai, M. A. (2020). Sensitivity of remote sensing-based vegetation proxies to climate and sea surface temperature variabilities in Australia and parts of Southeast Asia. *International Journal of Remote Sensing*, *41*(22), 8631–8653. https://doi.org/10.1080/01431161.2020.1782509

Belhaj, F., Rachid, H., Abdessalam, O., Tariq, A., Abdeldjalil, B., Mohamed, B., Alzahrani, H., Mustafa, H., & El-Askary, H. M. (2025). Predicting precipitation and NDVI utilization of the multi-level linear mixed-effects model and the CA-markov simulation model. *Climate Services*, *38*, 100554. https://doi.org/10.1016/j.cliser.2025.100554

Berra, E. F., Fontana, D. C., Yin, F., & Breunig, F. M. (2024). Harmonized Landsat and Sentinel-2 Data with Google Earth Engine. *Remote Sensing*, *16*(15), 2695. https://doi.org/10.3390/rs16152695

Darmawan, Y., & Sofan, P. (2012). Comparison of the Vegetation Indices To Detect the Tropical Rain Forest Changes Using Breaks for Additive Seasonal and Trend (Bfast) Model. *International Journal of Remote Sensing and Earth Sciences (IJReSES)*, *9*(1), 40–49. https://doi.org/10.30536/j.ijreses.2012.v9.a1823

Gao, W., Zheng, C., Liu, X., Lu, Y., Chen, Y., Wei, Y., & Ma, Y. (2022). NDVI-based vegetation dynamics and their responses to climate change and human activities from 1982 to 2020: A case study in the Mu Us Sandy Land, China. *Ecological Indicators*, *137*, 108745. https://doi.org/10.1016/j.ecolind.2022.108745

Hafiz, A. A., Usman, F., Hidayat, A. R. T., & Zakiyah, D. M. (2025). Spatiotemporal Dynamics of Urban Sprawl Types in the Peri-Urban Area of Malang Municipality, Indonesia. *Urban Science*, *9*(8), 313. https://doi.org/10.3390/urbansci9080313

Hasyim, A. W., Sukojo, B. M., Anggraini, I. A., Fatahillah, E. R., & Isdianto, A. (2025). Urban Heat Island Effect and Sustainable Planning: Analysis of Land Surface Temperature and Vegetation in Malang City. *International Journal of Sustainable Development and Planning*, *20*(2), 683–697. https://doi.org/10.18280/ijsdp.200218

Johnson, M. C., Reich, B. J., & Gray, J. M. (2021). Multisensor Fusion of Remotely Sensed Vegetation Indices Using Space-Time Dynamic Linear Models. *Journal of the Royal Statistical Society Series C: Applied Statistics*, *70*(3), 793–812. https://doi.org/10.1111/rssc.12495

Khallef, B., & Zennir, R. (2023). Forest cover change detection using Normalized Difference Vegetation Index in the Oued Bouhamdane watershed, Algeria - A case study. *Journal of Forest Science*, *69*(6), 254–265. https://doi.org/10.17221/192/2022-JFS

Khan, M. M. H., Mustafa, M. R. U., Hossain, M. S., Shams, S., & Julius, A. D. (2023). Short-Term and

Long-Term Rainfall Forecasting Using ARIMA Model. *International Journal of Environmental Science and Development*, *14*(5), 292–298. https://doi.org/10.18178/ijesd.2023.14.5.1447

Khan, M. S., Akter, A., Khan, I., Aguila, L. C. R., Akter, L., Yang, M., Li, X., & Li, Y. (2025). Assessing long term impact of regional climate and human activities on vegetation greenness dynamics in Sundarbans. *Ecological Informatics*, *85*, 102984. https://doi.org/10.1016/j.ecoinf.2024.102984

Kliengchuay, W., Phonphan, W., Niampradit, S., Kiangkoo, N., Srimanus, W., Niemmanee, T., Arunplod, C., Wen, B., Guo, Y., Herbreteau, V., & Tantrakarnapa, K. (2025). Variation of vegetation cover and the relationship with land surface temperature across Thailand (2007 to 2022). *Scientific Reports*, *15*(1), 40847. https://doi.org/10.1038/s41598-025-13018-y

Le, T. (2023). Increased impact of the El Niño–Southern Oscillation on global vegetation under future warming environment. *Scientific Reports*, *13*(1), 14880. https://doi.org/10.1038/s41598-023-41590-8

Li, S., Xu, L., Jing, Y., Yin, H., Li, X., & Guan, X. (2021). High-quality vegetation index product generation: A review of NDVI time series reconstruction techniques. *International Journal of Applied Earth Observation and Geoinformation*, *105*, 102640. https://doi.org/10.1016/j.jag.2021.102640

Liu, E., Zhou, G., Lv, X., & Song, X. (2024). Precipitation controls the time-lag and cumulative effects of hydrothermal factors on the end of the growing season in a semi-arid region of China. *Frontiers in Plant Science*, *15*, 1483452. https://doi.org/10.3389/fpls.2024.1483452

Lykhovyd, P., Vozhehova, R., & Averchev, O. (2024). Using Remote Sensing Normalised Difference Vegetation Index to Rec-ognise Irrigated Croplands via Agroland Classifier Application. *Visnyk of V.N. Karazin Kharkiv National University, Series Geology. Geography. Ecology*, *61*(61), 223–233. https://doi.org/10.26565/2410-7360-2024-61-18

Mahyuddin, A. A., & Arif, S. (2025). International Journal of Engineering and Science Applications Spatial Analysis of Vegetation Condition in the El Nino Phase of 2023 in Parangloe District , Gowa Regency. *International Journal of Engineering and Science Applications*, *12*(1), 35–40. https://doi.org/10.20956/ijesca.v0i0.6442

Marra, F., Armon, M., & Morin, E. (2022). Coastal and orographic effects on extreme precipitation revealed by weather radar observations. *Hydrology and Earth System Sciences*, *26*(5), 1439–1458. https://doi.org/10.5194/hess-26-1439-2022

Meviana, I., & Sari, U. A. (2017). Pemetaan Daerah Rawan Longsor Lahan Di Kecamatan Dau, Kabupaten Malang Dengan Menggunakan Pendekatan Geomorfolog. *JPIG (Jurnal Pendidikan Dan Ilmu Geografi)*, *2*(2), 127–134. https://doi.org/10.21067/jpig.v2i2.2493

Naicker, R., & Mutanga, O. (2024). Estimating high-density aboveground biomass within a complex tropical grassland using Worldview-3 imagery. *Environmental Monitoring and Assessment*, *196*(7), 12476. https://doi.org/10.1007/s10661-024-12476-7

Pambudi, P. A., Anggraeni, P. D., & ... (2024). Malang City Growth Dynamics and Implications for Environmental Aspects. *Regional Planning and Development Journal*, *1*(1), 4–20. Retrieved from https://journal-iasssf.com/index.php/IJOESAM/article/view/1178%0Ahttps://journal-iasssf.com/index.php/IJOESAM/article/download/1178/941

Permata, R. P., Ni'mah, R., & Dani, A. T. R. (2024). Daily Rainfall Forecasting with ARIMA Exogenous Variables and Support Vector Regression. *Jurnal Varian*, *7*(2), 177–188. https://doi.org/10.30812/varian.v7i2.3202

Raj, D. K., & Gopikrishnan, T. (2023). Machine learning models for predicting vegetation conditions in Mahanadi River basin. *Environmental Monitoring and Assessment*, *195*(12), 1401. https://doi.org/10.1007/s10661-023-12006-x

Ramdani, F., Setiani, P., & Sianturi, R. (2024). Towards understanding climate change impacts: monitoring the vegetation dynamics of terrestrial national parks in Indonesia. *Scientific Reports*, *14*(1), 18257. https://doi.org/10.1038/s41598-024-69276-9

Rustanto, A., & Booij, M. J. (2022). Evaluation of MODIS-Landsat and AVHRR-Landsat NDVI data fusion using a single pair base reference image: a case study in a tropical upstream catchment on Java, Indonesia. *International Journal of Digital Earth*, *15*(1), 164–197. https://doi.org/10.1080/17538947.2021.2018057

Safa, M., Kheirkhah Zarkesh, M., Ejlali, F., & Farsad4, F. (2021). The Spatial Autocorrelation between Precipitation and Vegetation Indices in the Bandar Abbas Basin. *International Journal of Scientific Research and Management*, *9*(12), 199–214. https://doi.org/10.18535/ijsrm/v9i12.fe1

Suhadi, Iskandar, I., Supari, Irfan, M., & Akhsan, H. (2023). Extreme Drought Assessment in Sumatra-Indonesia Using SPI and EDI. *Science and Technology Indonesia*, *8*(4), 691–700. https://doi.org/10.26554/sti.2023.8.4.691-700

Suud, H. M., & Kusbianto, D. E. (2024). Exploring El

Nino effects on agricultural area using Landsat images analysis: A case study in Bondowoso Regency, Indonesia. *SAINS TANAH - Journal of Soil Science and Agroclimatology*, *21*(2), 126. https://doi.org/10.20961/stjssa.v21i2.85190

Syaifullah, M. D., Purwandani, A., Kudsy, M., Tukiyat, T., S., S., E., A., Widodo, F. H., Bahri, S., & Muktiyono. (2025). Spatiotemporal analysis of rainfall variability using satellite precipitation in watersheds. *Global Journal of Environmental Science and Management*, *11*(3), 1143–1162. https://doi.org/10.22034/gjesm.2025.03.15

Trevisiol, F., Mattivi, P., Mandanici, E., & Bitelli, G. (2024). Cross-Sensors Comparison of Popular Vegetation Indexes From Landsat TM, ETM=, OLI, and Sentinel MSI for Time-Series Analysis Over Europe. *IEEE Transactions on Geoscience and Remote Sensing*, *62*, 1–16. https://doi.org/10.1109/TGRS.2023.3343071

Unsha, F. A., Rasnovi, S., & Dahlan. (2025). Application of Remote Sensing for Mapping Vegetation Density Using Normalized Difference Vegetation Index (NDVI) in Langsa City Mangrove Forest. *Jurnal Penelitian Pendidikan IPA*, *11*(7), 738–745. https://doi.org/10.29303/jppipa.v11i7.11530

Uribe, M. R., Sierra, C. A., & Dukes, J. S. (2021). Seasonality of Tropical Photosynthesis: A Pantropical Map of Correlations With Precipitation and Radiation and Comparison to Model Outputs. *Journal of Geophysical Research: Biogeosciences*, *126*(11), 2020 006123. https://doi.org/10.1029/2020JG006123

Waqas, M., Humphries, U. W., & Hlaing, P. T. (2024). Time series trend analysis and forecasting of climate variability using deep learning in Thailand. *Results in Engineering*, *24*, 102669. https://doi.org/10.1016/j.rineng.2024.102997

Wingate, V. R., Phinn, S. R., & Kuhn, N. (2019). Mapping precipitation-corrected NDVI trends across Namibia. *Science of The Total Environment*, *684*, 96–112. https://doi.org/10.1016/j.scitotenv.2019.05.158

Xue, J., & Su, B. (2017). Significant Remote Sensing Vegetation Indices: A Review of Developments and Applications. *Journal of Sensors*, *2017*, 1–17. https://doi.org/10.1155/2017/1353691

Yan, K., Gao, S., Yan, G., Ma, X., Chen, X., Zhu, P., Li, J., Gao, S., Gastellu-Etchegorry, J.-P., Myneni, R. B., & Wang, Q. (2025). A global systematic review of the remote sensing vegetation indices. *International Journal of Applied Earth Observation and Geoinformation*, *139*, 104560. https://doi.org/10.1016/j.jag.2025.104560

Yuniasih, B., Harahap, W. N., & Wardana, D. A. S. (2023). Anomali Iklim El Nino dan La Nina di Indonesia pada 2013-2022. *AGROISTA : Jurnal Agroteknologi*, *6*(2), 136–143. https://doi.org/10.55180/agi.v6i2.332

Zehri, S., Yulihastin, E., Marpaung, F., Adiputra, A., Mushoddik, Purwadani, N. N., & Gammamerdianti. (2025). Diverse impact of 2023 El Niño on weather patterns over the Indonesian Maritime Continent. *Journal of Southern Hemisphere Earth Systems Science*, *75*(2), 25005. https://doi.org/10.1071/ES25005